Final Scientific/Technical Report
A PORTABLE ION-ENERGY DIAGNOSTIC FOR
TRANSFORMATIVE ARPA-E FUSION R&D
Contract No. DE-AC02-09CH11466

Report No.	PPPL-2023_248
OSTI ID	1992496
Work Authorization No.	18/CJ000/13/03
Sponsoring Agency	USDOE, Advanced Research Project Agency – Energy (ARPA-E)
Lead Recipient	Princeton Plasma Physics Laboratory
Project Team Members	Princeton Plasma Physics Laboratory
Project Title	A portable ion-energy diagnostic for transformative ARPA-E Fusion R&D
Program Director	Dr. Scott Hsu, Dr. Robert Ledoux
Principal Investigator	Dr. Samuel Cohen
Contract Administrator	Marie Iseicz
Date of Report	03/15/2023
Reporting Period	03/19/2019 - 12/31/2021

Acknowledgements

Table of Contents

Public Executive Summary

The Princeton Plasma Physics Laboratory seeks to develop a diagnostic to measure the energy distribution of ions (IED) in innovative confinement concept devices being investigated under ARPA-E grants. The Princeton Field-Reversed Configuration (PFRC) fusion project, one of those innovative devices, aims to develop small, simple, and clean fusion power generators in the 1–10 MW "micro-reactor" class. The PFRC explores a new approach to fusion power-generation design, prioritizing low radioactivity and modular units of MW_e-scale power output. The team's proposed power plant design provides a small footprint for a compact, potentially transportable energy source that is fully deployable and emissions-free. A critical diagnostic to accomplish this mission and to test the theory of ion heating necessary for fusion in PFRC reactors is called a stripping-cell ion-energy analyzer (SC-IEA), the subject of this effort.

The PFRC concept uses an innovative method called odd-parity rotating-magnetic-field (RMF_o) predicted to heat ions and electrons to fusion-relevant energies and to drive electrical currents in the plasma, producing magnetic fields in the plasma that would confine and stabilize the plasma. The high-beta (β, ratio of plasma pressure to magnetic pressure) PFRC configuration is essential for achieving the high plasma ion temperatures needed for fusion of advanced fusion fuels, ones that produce little to no radioactivity at relatively modest magnetic fields. Low radioactivity reduces the required shielding thickness so that the reactor could potentially fit onto a truck, eases regulations and siting restrictions, and allows people to perform regular work relatively close by.

The goals of this project are to design, fabricate, and calibrate an SC-IEA diagnostic for studies of the PFRC-2 core physics, leading to the rapid development of a proof-of-concept machine. The PFRC-2 holds the world record for stable field-reversed configuration plasma duration. Upgrades for the PFRC-2 were intended to increase fuel density to the 10^{13} cm^{-3} range and reproducible electron and ion heating, both to above the 100 electron-Volt (eV) range. This requires increases in the radio-frequency (RF) forward power and magnetic field strength (B), as well as the application of sophisticated diagnostics to measure plasma temperature. In the experimental-results section we shall describe PFRC-2 experiments that resulted in electron temperatures above 100 eV, the presence of hotter minority electron populations, as well as plasma densities greater than 10^{13} cm^{-3}. Forward RF power was increased from 25 kW to 110 kW and the central magnetic field strength, B(0,0), was increased from 80 to 350 G. Covid delays and technical difficulties, the latter precluding RF operations at the lower frequency required for ion heating in the PFRC-2, prevented us from installing the SC-IEA and reaching the ion heating milestone. After this grant expired, we solved the technical difficulties and reached the required lower RMF frequency.

Initial targeted markets for the 1 to 10 MW PFRC-type reactors are high-value niche applications such as military forward power and space propulsion. In these areas, the PFRC will not need to compete in cost *per* kW and the needed helium-3 can be purchased. Helium-3 is found in nature and produced as a byproduct from several commercial processes. As more helium-3 becomes available, additional markets, such as emergency power, can be addressed. A two-reactor system is envisioned with moderately radioactive D-D breeder reactors serving as a source of helium-3 for ultra-clean reactors which would then provide cost-competitive

contributions to the electrical grid. Multiple PFRC-type modules could be used together for higher power, commercial, distributed power generation.

1. Project Accomplishments and Objectives

This award allowed Princeton Plasma Physics Laboratory to demonstrate several key objectives. The focus of the project was on developing and calibrating an ion energy diagnostic suitable for measuring the IED within the PFRC-2 plasma as it entered the ion heating parameter regime. Successful achievements included: designing the apparatus, ordering the components, assembling the components, achieving the required vacuum conditions, and calibrating the SC-IEA with an ion beam. Our progress on the final objectives – installing and operating the SC-IEA on the PFRC-2, with operations funded under a separate grant – was limited by the difficulty in lowering the operating frequency of the PFRC-2's RMF_o system, an effort supported by another grant, and by Covid restrictions.

The original tasks and milestones and final ones are presented in Figures 1a and 1b.

Our project was critically impacted by COVID. The Princeton Plasma Physics Laboratory was closed for many months and once it reopened there were severe restrictions on personnel allowed in each lab space. This slowed down procurement and limited the time available for diagnostic assembly and testing. As a result of the impacts, we had a schedule extension and budget increase. Even so, we were not able to meet the final project milestone, to install and operate the SC-IEA on the PFRC-2 and other ARPA-E innovative confinement concept devices.

Figure 1a: Original Project Milestones and Schedule.

Tasks		Milestones and Deliverables											
M1.0	**Go/No-Go: Refine tasks and milestones**	G/N	1	1	♦								
M1.1	**Go/No-Go: Refine designs for system calibration and operation**	G/N	1	1	♦								
M1.2	Assemble and calibrate SC-IEA		1	3		Δ							
M1.3	Install on PFRC-2		3	3		Δ							
M1.4	**Go/No-Go: Technical data agreement**	G/N	1	3		Δ							
M2.1	**Go/No-Go: Operations on PFRC-2**	G/N	3	3		♦							
M2.2	At $P_{RMF} < 100$ kW, $\Omega_{RMF}/\omega_{ci} \sim 10$		3	3		Δ							
M2.3	At P_{RMF} to 200 kW, $\Omega_{RMF}/\omega_{ci} < 2$		4	5					Δ				
M2.4	Submit papers to peer-reviewed journal		4	6							Δ		
M3.1	**Go/No-Go: Operations on HIT-SI**	G/N	5	5						♦			

	devices											
M3.2	Install SC-IEA on HIT-SI3; commence operations		5	6						Δ		
M3.3	Operations on HIT-SI3		6	7							Δ	
M3.4	Operations on HIT-SIU, high power		7	8								Δ
M3.5	Submit papers to peer-reviewed journal		6	8								Δ

Figure 1b: Final Project Milestones.

Project Schedule

WBS	Task/Milestone Title	G/N	Start	End	Quarters 1 2 3 4 5 6 7 8
M1.0	Go/No-Go: Refine tasks and milestones	v	1	1	
M1.1	Go/No-Go: Refine designs for system calibration and operation	v	1	1	
M1.2	Assemble and calibrate SC-IEA		3	3	
M1.3	Go/No-Go: Technical data agreement	v	3	3	
M2.1	Go/No-Go: Operations on PFRC-2	v	3	3	
M2.2	Obtain measurements at $P_{RMF} < 100$ kW, $\Omega_{RMF}/\omega_{ci} \sim 10$		3	3	
M2.3	Obtain measurements at P_{RMF} to 200 kW, $\Omega_{RMF}/\omega_{ci} < 2$		5	5	
M2.4	Submit papers to refereed journals		6	6	
M3.1	Go/No-Go: Operations of the HIT-SI devices	v	5	5	
M3.2	Install the SC-IAE on HIT-SI3/U and initiate operations		6	6	
M3.3	Operations on HIT-SI3/U device		8	8	
M3.4	Submit papers to refereed journals		8	8	

☐ Completed

▨ Removed

Descriptions of the milestones are summarized here:

Table 1: Key Technical Milestones and Deliverables

Task 1: Refine tasks and milestones 1.1 Refine designs for system calibration and operation	M1.1 Refine designs for system calibration and operation **Actual Performance:** The SC-IEA design was finalized and its placement on the PFRC-2 was selected in Q1. Test-particle modeling was performed of the IED and EED expected in the PFRC-2.
1.2 Assemble and calibrate the SC-IEA	M1.2 Assemble and calibrate the SC-IEA **Actual Performance:** Due to Covid delays, all parts were not ordered until Q3 and assembly not completed until Q4. A request for continuation funding was submitted to DOE. Approval was received in Q6. After the SC-IEA was assembled, calibrations were performed in Q4-8.
1.3 Technical data agreement	M1.3 Technical data agreement **Actual Performance:** Initial communication with CTFusion at APS DPP in 2019-OCT indicated no high-level issues. In Q7 it was concluded that no signed technical data agreement was needed.

5

Task 2: Operations on the PFRC-2	M2.2 Obtain measurement at $P_f < 100$ kW and $\Omega_{RMF}/\omega_{ce} \sim 10$
2.2 Obtain measurement at $P_f < 100$ kW and $\Omega_{RMF}/\omega_{ce} \sim 10$	**Actual Performance:** PFRC-2 operations were performed at 105 kW and. $\Omega_{RMF}/\omega_{ce} \sim 10$. Operations were performed with 5 different gases: H_2; D_2, He, Ne, and Ar. Densities exceeding 5 x 10^{13} cm^{-3} were achieved in Q:5-8. Measurements of T_e *via* Thompson scattering were not successful. Later measurements by soft X-ray emission revealed average energies in excess of 100 eV.
2.3 Obtain measurement at $P_f \sim 200$ kW and $\Omega_{RMF}/\omega_{ce} < 2$.	M2.3 Obtain measurement at $P_f \sim 200$ kW and $\Omega_{RMF}/\omega_{ce} < 2$. **Actual Performance:** Delays in reducing the RMF precluded operation at these powers and frequency ranges.
2.4 Submit articles to journals	M2.4 Submit articles to refereed journals **Actual Performance:** By Sept 2022, 11 papers related to this effort were submitted to refereed journals. By the beginning of 2023, all were published.
Task 3: Operations on HIT-SI device	M3. Operations on the HIT-SI device **Actual Performance:** All activities on the HIT-SI device were canceled

2.   Project Activities
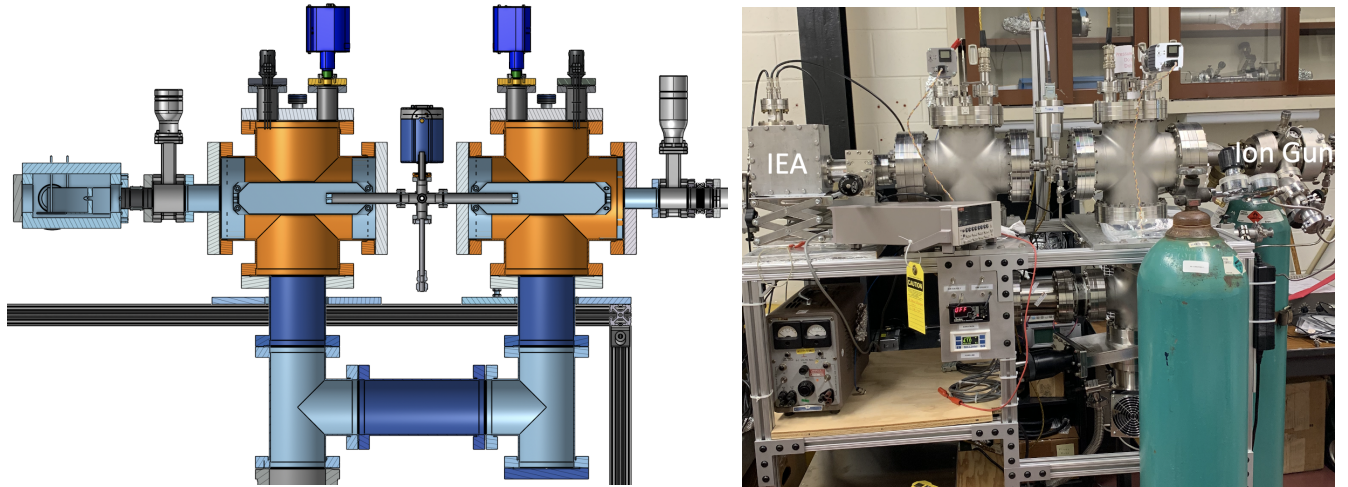
2.1 Diagnostic design and construction

Figure 2. SC-IEA vacuum system as designed (left) and as constructed (right).

The diagnostic design, see figure 2 (left), showed four sections: two pumped chambers (orange colored), the stripping cell between them, and the ion energy analyzer (IEA)/detector section (far left). The PFRC-2 would be located to the right. For the calibrations, a PHI ion gun was placed at the far right. Pumping is provided by a turbopump and by non-evaporable getters located in the two pumped chambers. These achieved a base pressure of 10^{-8} T. With the expected gas load from the stripping cell and from the PFRC-2, the pressure is predicted to rise to 10^{-5} T. The as-constructed SC-IEA, without the IEA installed, is shown in the picture on the right.

2.2 Energy Analyzer Subsystem

An IEA previously used at PPPL by R. Kaita was obtained, see figure 3, and its mechanical and electrical characteristics measured by N. Notis and D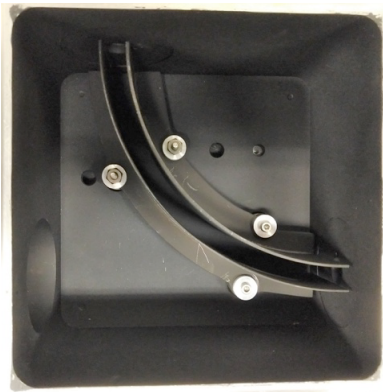. Singh. Sketches of the IEA are shown in figure 4. Figure 4a) is the CAD model of the IEA curved plates for calculating the electric field inside the IEA. As seen in figure 4a), the IEA is a pair of electrically biased plates of cylindrical geometry, subtending 90°. An electrostatic IEA of such shape transmits ions of the selected energy, E, (± energy resolution), independent of the ion mass. The outer plate has a mesh-covered hole (highlighted by the blue rectangle and magnified in the upper right sketch, figure 4b)) to allow alignment of the IEA system using a light beam extending from the PFRC-2. The IEA's energy range is ~ 0.1 to 2 keV with a calculated and measured energy resolution of $\Delta E/E \sim 7\%$.
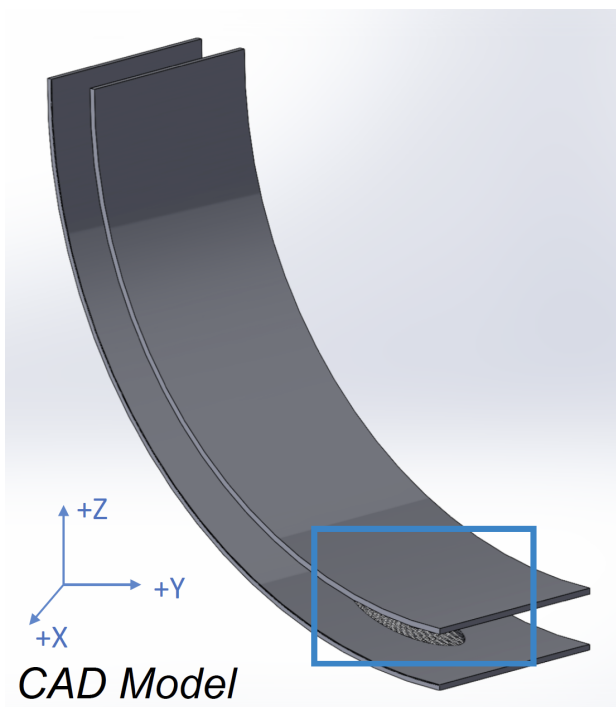
Figure 3. Photo of curved-plated IEA used.

Figure 4b). Magnified CAD model of mesh.

Figure 4a). CAD model of the IEA's curved plates. A metal mesh covers a hole in the outer plate. The hole is used for alignment purposes.
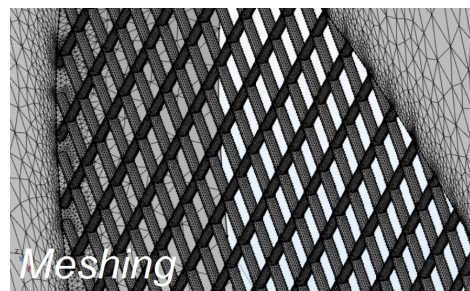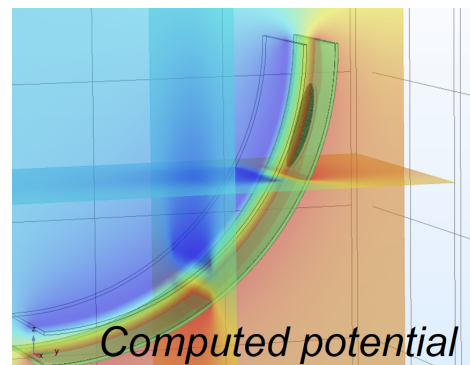
Figure 4c). Computed electrical potential created by DC biasing of the IEA's curved plates.
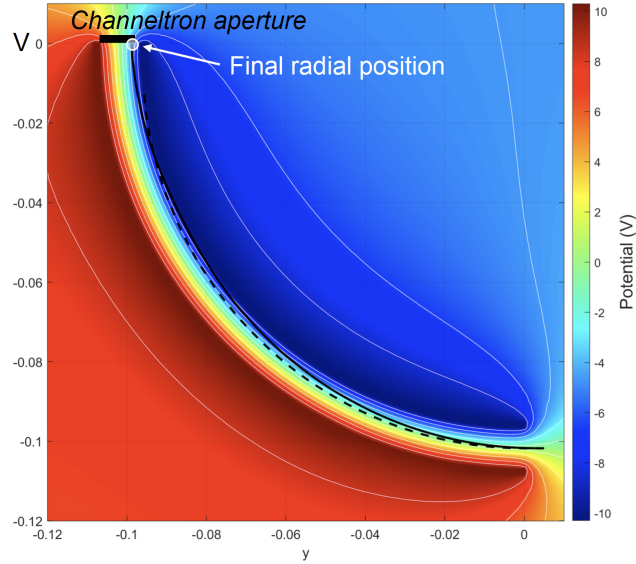
Figure 5. Location of Channeltron detector at the exit of the IEA's curved-plate region. The Channeltron converts the transmitted ions – a trajectory is represented by the dashed line – to an electrical current which is amplified then displayed on a digital oscilloscope (DSO), see figure 6.
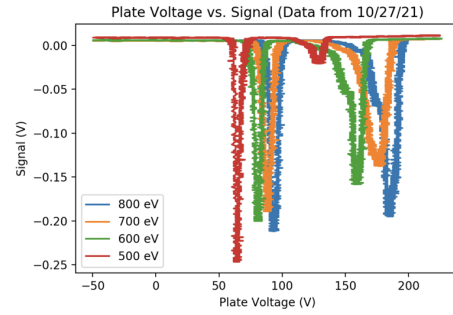

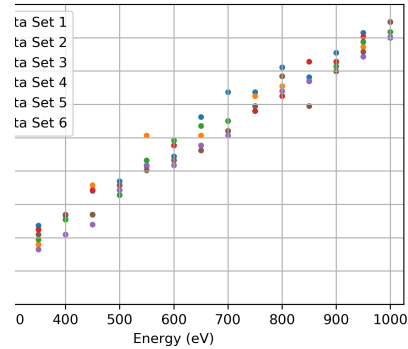**Figure 6.** Detected signal for 4 ion gun energies as functions of the voltage applied to the curved plates.

Figure 7. Ion energy *vs* voltage applied to IEA.

Ions, with either Ar or H_2 fill gas flowed into the PHI ion gun, were generated in the PHI ion gun with a set voltage applied to its acceleration grids. The ion beam was directed through the SC-IEA system. No gas was needed in the SC since the beam particles were already ionized. Figure 6 shows the detected signal for 4 values of the PHI acceleration (accel) grid voltages, 500, 600, 700, and 800 Volts. (The ion beam has a higher energy than that applied to the accel grids by ~ 100 eV because of bias applied to the ionization region in the ion gun.) Higher energy peaks are seen in the applied voltage region 120 -200 V and are attributed to doubly ionized ions formed in the PHI gun. These are not likely due to the fill gas since they are sometimes seen with H_2 fill gas. A likely source are molecules released in the source by outgassing caused by the temperature rise created by the hot filament of the ion source. Figure 7 is a summary of the data taken: peak location for each ion gun accel setting *vs* voltage applied to the plates. Ion beams with energies below 200 eV are not possible with the PHI ion gun.

2.3 Measurement of neutral density in the PFRC-2

Under the auspices of the Princeton Collaborative Low Temperature Plasma Research Facility (PCRF), a two-photon laser-induced-fluorescence (TALIF) diagnostic, constructed and operated by Dr. A. Dogariu (Princeton University), was used to measure the density of Hº and Krº in PFRC-2 plasmas. Knowledge of the Hº density is important for determining the absolute density of warm ions detected by the SC-IEA.

The TALIF diagnostic achieved time and spatial resolutions of 10 µs and 1 mm respectively

and a minimum detectable H^o density less than 10^{10} cm^{-3}. Knowledge of the neutral density is critical to assess and control plasma current loss and particle and energy confinement in present-day and fusion-reactor devices. Strong radial and temporal variation of the neutral density are shown in figures 1 (for Kr^o) and 2 (for H^o). Simulations of these were performed using the DEGAS code.
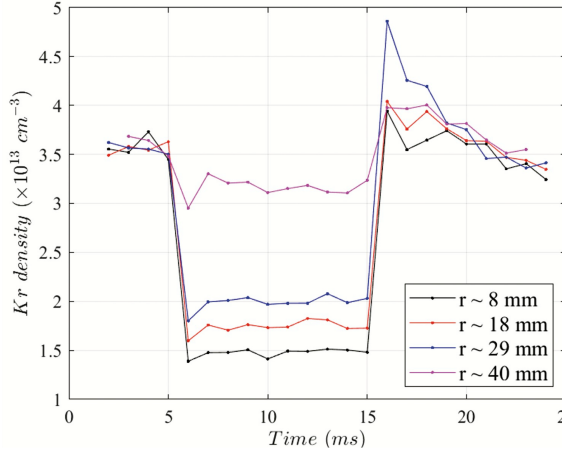

Figure 8. Time dependence of Kr^o density at 4 locations *vs* time. 10-ms-duration RMFo-heated discharge.
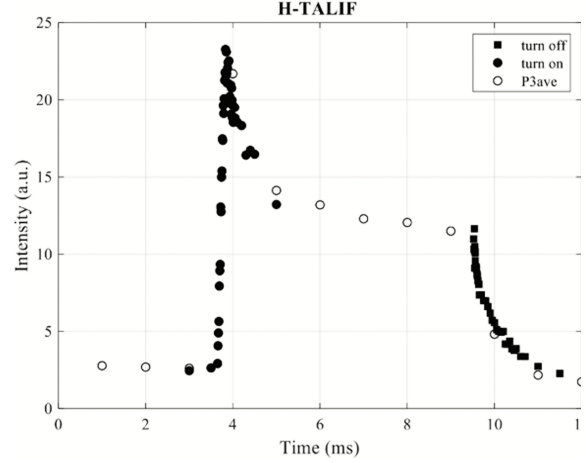

Figure 9. Central H^o density *vs* time in 6-ms duration RMF_o-heated discharge.

2.4 Achievement of higher plasma density

By increasing the axial magnetic field strength from 100 to 350 G, increasing the RMFo power to 100 kW, and using higher mass fill gases, higher density plasmas were achieved in the PFRC-2. The maximum density increased with the RMF_o power, initial axial magnetic field, and atomic mass unit (amu) of the fill gas. 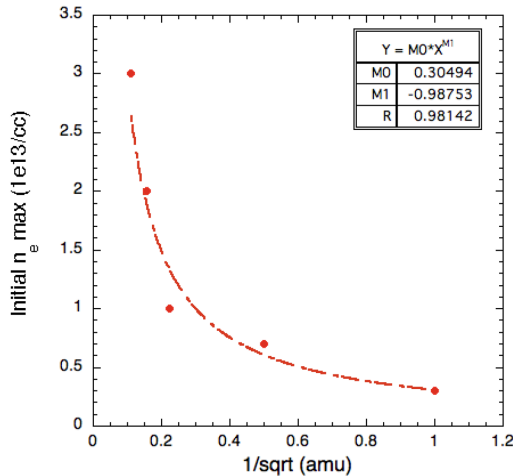Data taken at taken at 50 kW of forward RMFo power, P_f, and an axial field of 150 G are shown in Figure 10, under the assumption that the plasma radius equaled that of the internal flux conservers, 8 cm. The inferred density increases inversely to the actual plasma radius. Densities achieved exceeded that stated in the milestones by more than a factor of 3.

The $(amu)^{-1/2}$ dependence of maximum density indicates losses through a sheath at the ion sound speed. The higher power required at higher B to densify, Figure 12, can be interpreted as a β effect, that is, the need for higher nT for FRC formation, see next section.

Figure 10. Maximum initial plasma density achieved *vs* $(amu)^{-0.5}$ of fill gas.

2.5 FRC start-up

FRC start-up is of critical importance to reactor-scale FRCs, particularly those used in mobile applications and off-the-grid. These FRCs must have their own stored energy sources to re-start the plasma after a shut-down, whether intentional or accidental. We observed that the RMF_o power needed to form an FRC plasma increased with the initial magnetic field strength and decreased with the amu of the fill gas. Studies were done on the time-dependence of plasma start-up as a function of fill-gas species and pressure, RMF_o power, and applied axial field. The time behavior of the line-average plasma density is shown in Figure 11 for three powers, 40.5, 51.5 and 59.2 kW at $B(0,0) = 150$ G and $P_f = 50$ kW. Two characteristic rise times are seen here and for every case we have studied. For the displayed data, the long characteristic rise time was in the range 30-50 μs, followed by a short characteristic time, in the range 4-6 μs. In other cases, the long characteristic time could exceed 1 ms. The proxy parameter chosen to assess the power/energy needed for plasma start-up was the time to reach ½ of the maximum initial density.
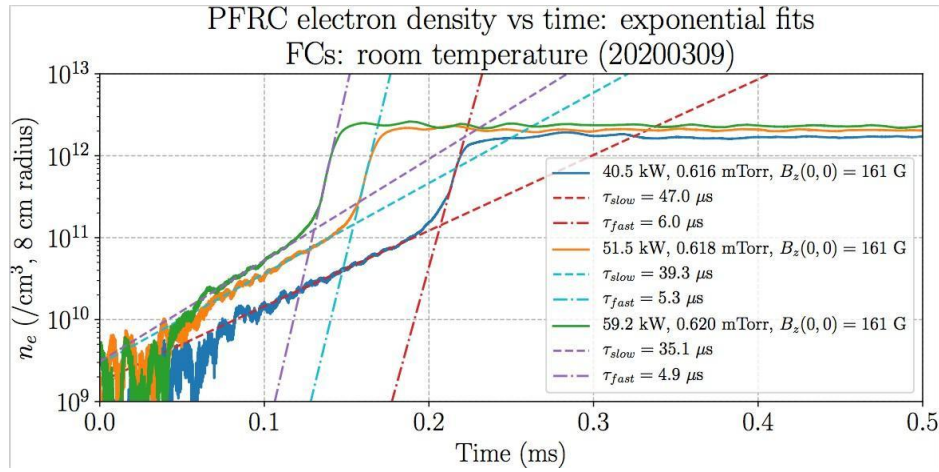

Figure 11. Time evolution of line-average (hydrogen) plasma density for three different RMF_o forward powers. The absorbed power was about 30% of the forward power.

Figure 12 shows that the breakdown time increases as the fill pressure falls and the field strength increases. The pressure dependence is consistent with the suggestion that collisions of electrons with neutrals are an important part of the breakdown process, specifically affecting power absorption and plasma heating. Modeling of the density rise during breakdown is consistent with ionization by electrons followed by a rapid contraction of the plasma column, as would happen as an FRC forms.
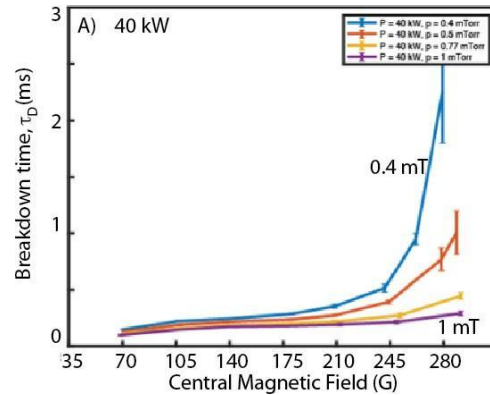

Figure 12. Breakdown time *vs* axial magnetic field strength for four different H_2 fill pressures: 0.4, 0.5, 0.77 and 1.0 mTorr.

2.6 Synthetic diagnostic to extract IED from energy-resolved charge exchange flux

Extracting the ion energy distribution (IED) from the energy-resolved charge exchange flux (CX) is far more complex in highly kinetic high-β plasmas than in low-β devices, like tokamaks, because of the strong dependence of the flux on the viewing position due to the different classes of orbits that exist in high-β plasma devices that have a null in the total magnetic field, hence the ratio of gyro-radii to machine size is of non-negligible value, 0.1 to 1. The three classes of orbits are cyclotron, betatron, and figure 8, see Figure 13. Only cyclotron orbits exist in tokamaks. We have written a code to guide the interpretation of the SC-IEA's CX signals and to determine the position of the SC-IEA to best measure the IED. Figure 14 shows a sample of the results.
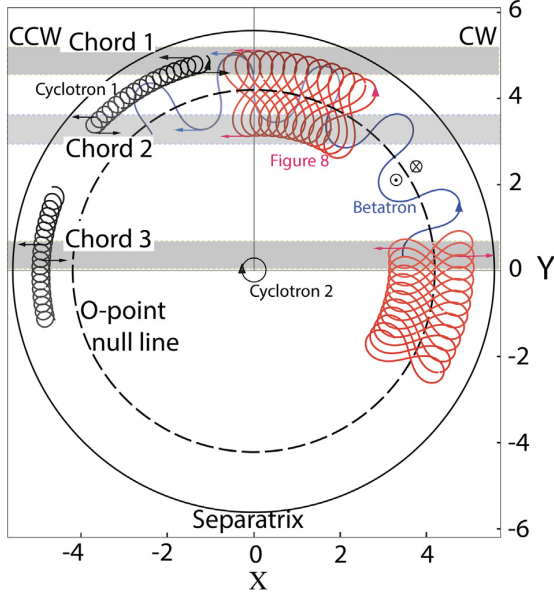

Figure 13. Sample trajectories of three orbit classes in FRC midplane. Different signal strengths and energy distributions would be measured by CX detectors viewing CW or CCW along the gray chords.
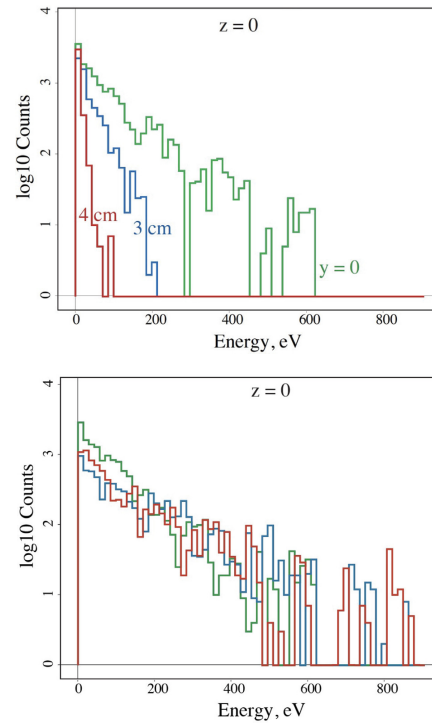

Figure 14. (top) IED seen by CW-viewing detectors along three lines-of-sight. (bottom) IED seen by CCW-viewing detectors along the same tangency lines-of-sight.

2.7 X-ray measurements for the electron energy distribution (EED)

Our present method for measuring the electron temperature (T_e) in the PFRC-2 relies on energy- resolving X-ray detectors (SDDs) of the pulse-height type. Because of the high flux of X-rays and VUV photons, pulse pile-up (PPU) may be a problem. Several methods were developed to avoid this artifact in our experiments, allowing the energy range of the PFRC-2's SDD to be extended down to 120 eV. (Intrinsic noise in the Peltier-cooled detector peaks at 10^3 counts *per* second at 30 eV and falls to below one count *per* second at 120 eV.) The PPU-reduction methods included: using apertures in front to the SSD to reduce the X-ray flux and check the scaling of flux with aperture area; shortening the SDD peaking time; developing

an algorithm that allowed removal of PPU-generated artifacts; and reducing the transmission of UV photons to the detector by inserting an 0.85-µ Mylar filter between the plasma and the SDD. Figures 15-17 (3-7-2023) are sample results of X-ray spectra from 4-ms-duration Ar discharges with absorbed RMF_o power of ~ 30 kW. The line-average density was 7 x 10^{12} cm^{-3}, assuming an 8-cm radius uniform density plasma. The average energy increases with increasing magnetic field from 110 eV to 300 eV as the B(0,0) was increased from 140 to 250 G.
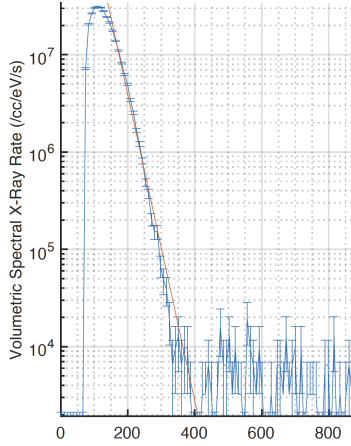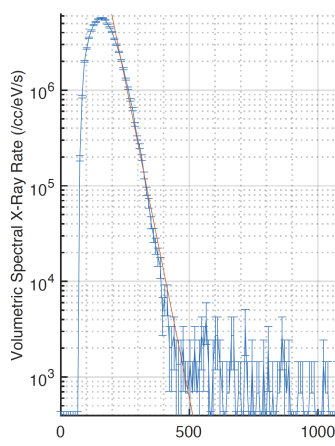

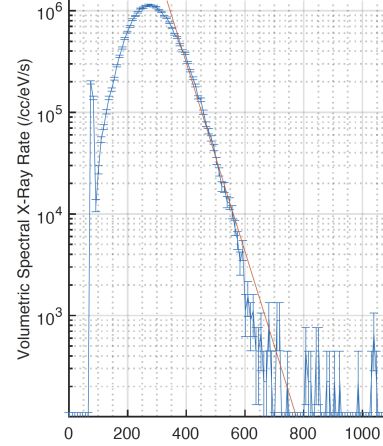**Figure 15.** B(0,0) = 140 G.   **Figure 16.** B(0,0) = 200 G.   **Figure 17.** B(0,0) = 250 G.

3.   Publications describing this work

1. A.H. Glasser and S.A. Cohen, Interpreting ion-energy distributions using charge exchange emitted from deeply kinetic field-reversed-configuration plasma. *Phys Plasmas* **29**, 052508 (2022). DOI: 10.1063/5.0089430

2. A.H. Glasser and S.A. Cohen, "Simulating single-particle dynamics in magnetized plasmas: The RMF code," *Rev. Sci. Instrum*. **93**, 083506 (2022). DOI: 10.1063/5.0101665

3. Arthur Dogariu, S.A. Cohen, P. Jandovitz, E.S. Evans, S. Vinoth, and C.P.S. Swanson. A diagnostic to measure neutral atom density in fusion-research plasmas, *Rev. Sci. Instrum.* **93,** 093519 (2022). DOI: 10.1063/5.0101683

4. S.P. Vinoth, E.S. Evans, C.P.S. Swanson, E. Palmerduca, and S.A. Cohen. Evaluation of a collisional radiative model for electron temperature determination in hydrogen plasma, *Rev. Sci. Instrum.* **93,** 093503 (2022). DOI: 10.1063/5.0101676. Selected by AIP to appear in *AIP Publishing Showcase*.

5. C.A. Galea, C.P.S. Swanson, S.A. Cohen, and S.J. Thomas. Use of a Mylar filter to eliminate VUV pulse pileup in low-energy x-ray measurements, *Rev. Sci. Instrum. **93,*** 093531 (2022). DOI: 10.1063/5.0101712

6. N. Kafle, D. Elliott, B. Berlinger, Z. He, S. Cohen, Z. Zhang, and T.M. Biewer. Portable Diagnostic Package for Thomson scattering and Optical Emission Spectroscopy on Princeton Field-reversed Configuration (PFRC-2), *Rev. Sci. Instrum.* **93**, 113506 (2022). DOI: 10.1063/5.0101849

7. C.A. Galea, M. Paluszek, S.J. Thomas, and S.A. Cohen. The Princeton Field Reversed Configuration for Compact Nuclear Fusion Power Plants, *J. Fusion Energy* **42**, (2023). DOI: [10.1007/s10894-023-00342-2](#)

8. T. Ahsan, C.P.S. Swanson, T. Qian, T. Rubin, and S.A. Cohen. The pulse-pile-up tail artifact in pulse-height spectra, *Plasma* **6**, *58 (2023)*. DOI: [10.3390/plasma6010006](#)

Papers 2-6 were presented at the Diagnostics of High Temperature Plasma Conference, Rochester, NY (2022).

4.   Conference Papers

Our team has presented posters on the progress of this program at the 2019, 2020, 2021, 2022 APS DPP meetings. These are listed below.

DPP 2019 posters:
- E. S. Evans and S. A. Cohen, "Neutral density measurements on the PFRC-2"

- P. Jandovitz, C. Swanson, E. Palmerduca, and S. A. Cohen, "Visible light imaging of low-frequency oscillations in the PFRC"

- E. Palmerduca, S. Punjabi-Vinoth, G. Gonzalez Jusino, and S. A. Cohen, "Visible Spectroscopy and Collisional Radiative Models for PFRC-II"

- C. Swanson, B. Alessio, E. S. Evans, E. Palmerduca, and S. A. Cohen, "Recent X-ray results from the PFRC-2 experiment"

APS DPP 2020 posters (virtual)
- C. Swanson, "X-ray measurements of the PFRC-2 operating at high power and high field."

- S. Punjabi Vinoth, "Collisional-Radiative-Model Determination of Electron Temperature in PFRC-II Hydrogen Plasmas"

Similar presentations were made by Dr. Swanson and Dr. Vinoth at the US-Japan Compact Torus Workshop, virtual conference in January 2021.

APS DPP 2021 posters:
- S.P. Vinoth, E. Palmerduca, D. Elliot, N. Kafle, T. Biewer, Z. Hu, C.P. Swanson, E. Evans, A. Dogariu, S.A Cohen, "Inferring electron temperature in warm hydrogen plasmas using a collisional radiative model"

- H. Doucet, S.A. Cohen, A. Sefkow, A. Kish "A TriForce module for performing in-line Hydrogen spec- troscopy on the Princeton Re- versed Field Configuration"

- T. Ahsan, C.P. Swanson, S.A. Cohen, "The pulse-pile-up tail artifact in pulse-height spectra"

- M. Notis, A. Glasser, S.A. Cohen, S. Abe, "An Electrostatic Energy Analyzer and Gas Stripping Cell to Measure Ion Temperature in the PFRC-2"

- C. Biava, G. Wilkie, A. Dogariu, S.A. Cohen, "Modeling spatially resolved neutral atom densities in the PFRC-2 Using DEGAS 2"

APS DPP 2022 posters and presentations:

- C. Galea, S. Thomas, S. Vinoth, S.A. Cohen, and M. Paluszek, "Leveraging Public-Private Partnerships for the Development of PFRCs"
- S. P. Vinoth, E. Evans, E. Palmerduca, S.A. Cohen, "A trustworthy method to evaluate the Balmer line ratio to predict electron temperature using Collisional Radiative model for Hydrogen plasma in PFRC-2"
- C.A. Galea, S. Vinoth, S. J. Thomas, S.A. Cohen, "X-ray measurements of electron density and temperature in the PFRC-2"
- P. Hooda, S.A. Cohen "Thermoelectric generators to re-start FRC reactors"
- M. Kim, S. Thomas, S.A. Cohen, "Consideration of Vacuum Vessel Properties Required for PFRC-type Fusion Reactors"
- M. Demir, S.A. Cohen, "Kinetic simulations of the PFRC-2 using the VPIC code"

5.   Reports, websites, patents, outreach, and follow-on funding

Status Reports

Status reports were submitted quarterly and are available within ePic.

Media Reports

The following article was posted in the Proceedings of the National Academy of Sciences (PNAS), which described the PFRC in the context of other commercial fusion and FRC approaches:

M. Mitchell Waldrop, "Small-scale fusion tackles energy, space applications," January 28, 2020, DOI: 10.1073/pnas.1921779117

Invention Disclosures

None.

Patent Applications

There are no new patent applications derived from this contract.

Licensed Technologies

There are no licensed technologies.

Networks/Collaborations Fostered

We have developed many collaborations during the course of our ARPA-E award. One is with the U. Rochester team, led by Prof. Adam Sefkow, which is applying a modern particle-in-cell (PIC) code, TriForce, to first replicating the PFRC-1 results from the LSP code and then working on PFRC-2 scale simulations. A critical collaboration is with Princeton Satellite Systems, through their ARPA-E OPEN and INFUSE awards.

We collaborated with several of the Fusion Diagnostics awardees. This includes ORNL's portable Thomson Scattering diagnostic program run by Dr. Theodore Biewer, which

visited PPPL from mid-2021 through early 2022. UC-Davis, led by Dr. Neville Luhmann, Jr. had planned to bring their USPR diagnostic to the PFRC, however this was canceled due to COVID but is scheduled for FY 2023-24.

Websites Featuring Project Work Results

- The website https://w3.pppl.gov/ppst/pages/pfrc_papers.html contains all the published papers
- The website https://w3.pppl.gov/ppst/pages/ugrad_interns.html contains the reports of summer interns.
- Data from the PFRC-2 is posted on the website smb://samba.pppl.gov/projects/pfrc/data

Awards, Prizes and Recognition

Team members received a Thomas Edison Patent award in 2020 from the New Jersey Research & Development Council for prior PFRC-related inventions.

Student involvement

Students were heavily involved, providing essential engineering and scientific efforts in developing the SC-IEA diagnostic. Mr. E. Evans, a Princeton graduate student in the Plasma Physics program, provided the initial design and evaluation of the SC-IEA's capabilities. He identified the commercial components required, placed orders for them, and oversaw the SC-IEA's assembly. Mr. N. Notis, a Princeton undergraduate in the Physics department, participated in three ways, as a summer intern, writing a Junior paper, and, through his thesis work, providing a calibration of the SC-IEA's sensitivity and energy resolution. Mr. D. Singh, a Princeton undergraduate in the MAE department, made detailed measurements of the curved-plate energy-selection section and measured the energy resolution at high plate-voltage scan rates. Mr. C. Galea, then a Princeton graduate student in the MEA department, participated in the TALIF measurements.

Follow-On Funding

Princeton Satellite Systems, with PPPL as co-PI, was selected for two INFUSE awards in the 2022A cycle.

Table 6-1: Follow-On Funding Received

Source	Title or Contract	Funds Committed or Received
INFUSE 2022a	Evaluating RF antenna designs for PFRC plasma heating and sustainment (PPPL)	$300K federal funding
INFUSE2022a	Stabilizing PFRC plasmas against macroscopic low- frequency modes (PPPL)	$240K federal funding